Active vibration suppression in a suspended Fabry-Pérot cavity

Enrico S. Canuto, *Member, IEEE*, and Andrea Rolino, *student*

***Abstract*— This paper is concerned with active vibration suppression in a suspended Fabry-Pérot cavity, employed as force sensor in a thrust-stand, called *Nanobalance.* The Nanobalance aims to exploit sensitivity of in-vacuum Fabry-Pérot interferometers to sub-nanometric displacements in order to measure micro-thrusts with micronewton accuracy. The instrument has been conceived around an in-vacuum optical cavity embraced by two pendulums suspended to an athermic spacer. The objective of the paper is to suppress the beat motion around the pendulum natural frequency (>10Hz) without affecting the measurement bandwidth (<2 Hz) where thrust has to be measured. Beat motion arises because of small pendulum imbalances excited by ground noise. Relevant digital control strategies and experimental results will be presented and discussed.**

I. Introduction

This paper is concerned with active vibration suppression in a suspended Fabry-Pérot cavity, employed as force sensor in a thrust-stand, called *Nanobalance*, conceived and built by "G. Colonnetti" Metrology Institute, Alenia Spazio and Politecnico di Torino, Turin, Italy. Instrument, motivation and principles have been already presented at past ACCs ([2], see also [3]). The authors are responsible for instrument automation.

The Nanobalance aims to exploit sensitivity of in-vacuum Fabry-Pérot (FP) interferometers to sub-nanometric displacements. The instrument has been conceived around an in-vacuum optical cavity embraced by two pendulums suspended to an athermic spacer by flexible joints. By locking the frequency of the injected laser beam to the optical path length inside the cavity, the tunable laser frequency becomes proportional to cavity length perturbations and therefore to actual thrust under test. This is obtained by servoing the built-in frequency actuators (PZT ceramic, thermo-electric cooler) of the laser source to the interferometer signal, which is highly sensible to optical length and laser frequency detuning around multiples of the laser radiation half wavelength.

Under perfectly equal pendulums, the force balance would reach equilibrium in absence of a thrust under test and the cavity length would be kept constant although both pendulums were oscillating subject to ground noise. Actually, small differences in stiffness of the flexible joints as well as in mass and inertia might imbalance the instrument and generate a beat motion excited by ground accelerations. The spectral density of the beat motion is highly concentrated around the pendulum natural frequency (>10Hz), but spreads toward the measurement bandwidth (MBW<2 Hz), where becomes a source of measurement noise.

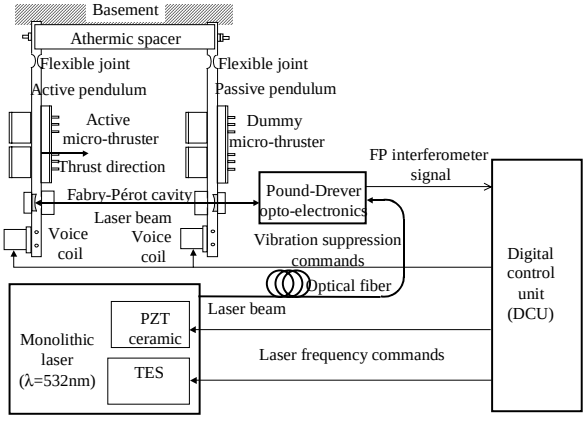

Fig. 1. Layout and block diagram of the instrument.

The objective of the paper is to suppress the beat motion around the pendulum natural frequency (>10Hz) without affecting the MBW (<2 Hz) where thrust has to be measured. The advantage is to greatly reduce the tuning range of the laser frequency actuators in charge of tracking the cavity length detuning within the MBW. In fact, the limited range of the fastest actuator (PZT) might be saturated by the beat motion under severe ground motion or because of sudden shocks, forcing measurement tests to be interrupted. The only drawback is the additional MBW noise of the actuator employed to suppress vibrations, one of the two voice coils (VC) mounted at the lower extremes of each pendulum. Therefore, vibration suppression has been designed and implemented as a backup solution of the default Nanobalance digital control.

This work was supported in part by a grant of Alenia Spazio, Turin, Italy.

E. S. Canuto is with Politecnico di Torino, Dipartimento di Automatica e Informatica, Corso Duca degli Abruzzi 24, 10129 Torino, Italy (phone: +39-011-5647026; fax: +39-011-5647099; e-mail: enrico.canuto@ polito.it).

A. Rolino is with Politecnico di Torino, Dipartimento di Automatica e Informatica, Corso Duca degli Abruzzi 24, 10129 Torino, Italy (e-mail: andrea.rolino@ polito.it).

The paper is organized as follows. Section 2 recalls Nanobalance principles and formulates the relevant control problems, essential to instrument performance. Section 3 treats Nanobalance actuators and sensor, giving emphasis to the interferometer sensor, peculiar to the instrument. Section 4 reports the digital control design centered around vibration suppression capability. Digital control is based on a discrete-time design model to be embedded in the control strategies in the form of a state observer and suitable digital filters apportioning the estimated disturbance to different actuators. Section 5 briefly reports experimental results.

II. Instrument Principle and Control Problems

A. Instrument principle

The force balance is made by two metallic plates, denoted with j=1,2 (*pendulums*), which should be equal in geometry and mass distribution. Their upper pivots, made by flexible joints, are kept at constant distance by an athermic spacer. The micro-thruster (MT) under test is mounted on the *active* pendulum, the left one in Fig. 1. To balance the active MT, a dummy one is mounted on the *passive* pendulum, the right one in Fig. 1. The vibration suppression actuators are mounted on the lower extreme of each pendulum.

Distance variations between pendulums are revealed by a FP interferometer, which is made by two optical reflectors mounted on the lower part of each plate. The visible radiation ($\lambda_0 = 532$ nm) of a monolithic laser (Nd-YAG crystal) is injected into the mirror cavity from one side. The optical radiation reflected by the cavity encodes the optical length variation ΔL as a phase variation of the reflected electromagnetic field. They can be revealed by a Pound-Drever electronics [5] only when the cavity length is kept close, although variable, to a resonance length

$$L(t) \simeq N\lambda(t)/2\,, \tag{1}$$

i.e. to an integer multiple N of the half-wavelength of the incident radiation. Replacing λ in (1) with the frequency $f(t) = c/\lambda(t)$ yields the constant product

$$L(t)\,f(t) \simeq Nc/2 = \text{constant}\,, \tag{2}$$

where c is the speed of light in vacuum. By differentiating (2) around a fixed resonant length $L_0 f_0 = Nc/2$, the *fundamental instrument equation* follows

$$e(t) = \Delta L(t)\,f_0 / L_0 + \Delta f(t)\,, \tag{3}$$

where Δf is the laser frequency variation to be actuated for keeping the cavity close to resonant condition (1) less a frequency error e.

By assuming superposition, cavity detuning ΔL and frequency detuning Δf can be decomposed into command and disturbance components as follows

$$\begin{aligned} \Delta L(t) &= \Delta L_t(t) + \Delta L_s(t) + \Delta L_v(t) = \Delta L_d(t) + \Delta L_v(t) \\ \Delta f(t) &= \Delta f_p(t) + \Delta f_t(t) + \Delta f_l(t) = \Delta f_u(t) + \Delta f_l(t) \end{aligned}\,, \tag{4}$$

where the following components can be distinguished.

1. ΔL_t is the component due to MT which is to be measured by the instrument, ΔL_s accounts for ground noise and ΔL_v is the result of the voice coil thrust. The first two components are collected into the cavity disturbance ΔL_d.
2. Δf_p and Δf_t are the frequency variations actuated by the laser built-in PZT and the temperature servo (TES), respectively; Δf_l is the free laser drift. The first two components are collected into the total actuated frequency Δf_u.

The instrument target is to measure the cavity detuning ΔL_t, due to active MT, from the frequency detuning Δf within the so-called measurement bandwidth (MBW). The latter encompasses a finite frequency region from a lower bound f_l to an upper bound f_h. Typical values from GOCE mission [3] are:

$$f_l = 0.1\ \text{mHz},\ f_h = 2\ \text{Hz}\,, \tag{5}$$

but here the lower bound will be extended to DC for control purposes, i.e. $f_l = 0$.

To retrieve the sole cavity detuning components $\underline{\Delta L}(t)$ within the extended MBW from DC to f_h, a digital low-pass filter $\mathbf{L}$ [1] has been designed [6]. The harmonic response (amplitude) of $\mathbf{L}$ and of the sensitivity $\mathbf{I}-\mathbf{L}$ are shown in Fig. 2. The design procedure of $\mathbf{L}$ is not reported here for sake of brevity.

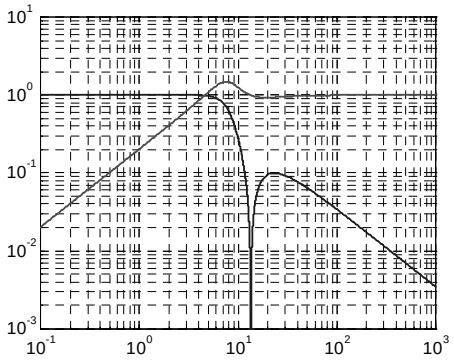

Fig. 2. Amplitude of the filter and sensitivity harmonic response.

B. Control problems

The key control problem is to look for a resonant

[1] The symbol $\mathbf{L}$ will be employed to denote the discrete-time (DT) response $y(i)$ of the filter in the form $y(i) = \mathbf{L}\cdot u(i)$ and the relevant Z-transform $\mathbf{L}(z)$.

condition (1) at some time t_0 and then to keep the resonance by forcing $e(t)$ close to zero in (3), thus making Δf proportional to ΔL as required by the instrument principle. Upon a suitable selection of the control time unit $T = 0.1$ ms, control problems can be formulated in the discrete-time domain, i denoting discrete time and $\Delta L(i)$ an anti-aliased sample of $\Delta L(t)$. They are:

3. *Interferometer lock-in:* to move the laser radiation frequency $f_l(t)$ until the actual cavity length $L(t)$ approaches a resonant length at t_0, i.e.

$$L(t_0) \cong L_0(N) = 2N/\lambda_0 = 2Nf_l(t_0)/c,\ f_0 = f_l(t_0) \quad (6)$$

4. *Cavity length tracking:* to make the laser command $\Delta f_u(i)$ to track and cancel the MBW components of $\Delta L_d(i)$ and $\Delta f_l(i)$, i.e.

$$\Delta f_u(i) = -\mathbf{L}\cdot\left(f_0\widehat{\Delta L}_d(i)/L_0 + \widehat{\Delta f}_l(i)\right), \quad (7)$$

the symbol $\widehat{\Delta L}$ denoting estimate. Canceling $\mathbf{L}\cdot\widehat{\Delta f}_l$ in (4) removes the laser drift from Δf. Canceling $\mathbf{L}\cdot\widehat{\Delta f}_d$ keeps the cavity locked and encodes the MBW cavity length detuning into Δf.

5. *Vibration suppression*: to suppress cavity beat motion through voice coil actuation, i.e.

$$\Delta L_v(i) = -(\mathbf{I}-\mathbf{L})\cdot\widehat{\Delta L}_d(i), \quad (8)$$

in order to reduce the command effort Δf_u of laser built-in actuators.

6. *Closed-loop stability:* to ensure the error $e(i)$ in (3) to be statistically bounded and asymptotically zero-mean. From (3), (7) and (8), the error $e(i)$ holds

$$\begin{aligned} e(i) &= f_0\hat{e}_d(i)/L_0 + \mathbf{L}\cdot\hat{e}_l(i) + (\mathbf{I}-\mathbf{L})\Delta f_l(i) \\ \hat{e}_d(i) &= \Delta L_d(i) - \widehat{\Delta L}_d(i),\ \hat{e}_l(i) = \Delta f_l(i) - \widehat{\Delta f}_l(i) \end{aligned} \quad (9)$$

Closed-loop stability must be ensured because the RHS of (9) will depend on $e(i)$ through estimation and modelling errors.

III. Control components

The section briefly reports actuators and sensor. Sensor response will be treated in some detail. Pendulum dynamics has been reported in [3].

A. Actuators

Actuator dynamics can be modelled as low-pass dynamics with finite DC gain and some dominant poles. PZT and voice coil dynamics are very fast (<0.1 ms), TES dynamics is quite slow (>1s). Their response can be assumed to be linear within command range as confirmed by experimental tests. Actuators data are shown in Table I.

TABLE I ACTUATORS DATA

Parameter	TES	PZT	VC
Range [MHz]	±5000	±250	±1.25
Time constant [s]	6	<0.0001	<0.0001

B. Interferometer sensor

The frequency error $e(t)$ defined in (3) is measured by an opto-electronics ([3], [5]) providing an output voltage *V(t)* which is different from zero only in a small region, the 'useful region', centered at a resonant cavity length. Cavity resonance can be defined either in length units or in frequency units, the latter as an integer multiple *N* of the so-called Free Spectral Range (FSR) defined by

$$F_0 = 0.5c/L_0 = 0.5 f_0\lambda_0/L_0 \cong 769 \text{ MHz} \quad (10)$$

The width of the useful region (Fig. 3) is about twice the modulation frequency $f_m \cong 25$ kHz applied to laser beam by the interferometer opto-electronics.

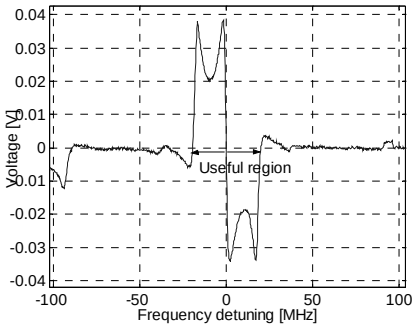

Fig. 3. Interferometer response and 'useful region'.

To keep the error $e(t)$ close to zero, the DCU must confine the output voltage within a much smaller region, the 'linear region', about one tenth of the useful region, where $V(t)$ undergoes a sharp zero-crossing and becomes monotonic and quasi proportional to $e(t)$. The interferometer response within this region holds

$$\begin{aligned} V(t) &= h(e(t)) = 2V_{\max}\left(e(t)/e_{\max}\right)/\left(1+\left(e(t)/e_{\max}\right)^2\right) \\ &\left|e(t)/e_{\max}\right| \le 1,\ e_{\max} \le 2.5 \text{ MHz} \end{aligned} \quad (11)$$

having denoted the region half-width with $e_{\max}$. When $|e(t)| < e_{\max}$, the interferometer is said to be locked-in; when $|e(t)| > f_m$, the interferometer is said to be locked-out. The voltage output corrupted by the opto-electronic noise is usually filtered to reduce noise aliasing. By denoting filter dynamics with $\mathbf{M}_s$, the sensor output $y(t)$ can be written as

$$y(t) = \mathbf{M}_s\cdot V(t) + v(t) = \mathbf{M}_s\cdot h(e(t)) + v(t). \quad (12)$$

IV. SOLUTION OF CONTROL PROBLEMS

A. The design model

The control problems of Section II.B are solved by a model/observer based methodology ([1], [3], [4]). Accordingly, control strategies are designed as output-to-state feedback (state observer feedback) and state-to-command feedback (feedback control) around a DT design model of the controllable dynamics and of the unknown/observable disturbance to be cancelled. In this paper only problems 2, 3 and 4 (tracking, vibration suppression and closed-loop stability) will be solved. Lock-in problem has been treated in [3].

1) Controllable dynamics.

The controllable dynamics is a multi-input dynamics modelling the available actuators: PZT, TES and VC.

1. PZT dynamics $\mathbf{M}_p = b_p$ is neglected, being faster than T, and simplified to the voltage-to-frequency gain b_p.
2. TES dynamics $\mathbf{M}_t(z) = b_t\beta_t\left((z-1)+\beta_t\right)$ is the slowest one and is approximated by a first order dynamics, according to experimental tests.
3. VC dynamics is neglected, but voice coils act on the cavity length through 2nd order pendulum dynamics tuned to mean resonance frequency $\underline{f} = 13.45$ Hz:

$$\mathbf{M}_v(z) = b_v\alpha_v \Big/ \left((z-1)^2 + \beta(z-1) + \alpha\right),\ \sqrt{\alpha} = 2\pi\,\underline{f}T \quad (13)$$

By denoting the actuator voltage commands with u_p, u_t and u_v, respectively, the DT frequency error $e(i)$ can be written from (3) and (4) as

$$\begin{aligned} e(i) &= \Delta f_p(i) + \Delta f_t(i) + \Delta f_v(i) + d(i) + \textstyle\sum_j \partial\mathbf{P}_j(\Delta f_j) \\ \Delta f_p(i) &= b_p u_p(i),\ \Delta f_t(i) = \mathbf{M}_t \cdot u_t(i) \\ \Delta f_v(i) &= \mathbf{M}_v \cdot u_v(i) = f_0 \Delta L_v(i)/L_0 \\ d(i) &= \Delta f_l(i) + f_0 \Delta L_d(i)/L_0 \end{aligned} \quad ,(14)$$

where $j = p,t,v$, $\partial\mathbf{P}_j(\Delta f_j)$ stands for the unmodelled dynamics of the actuator j and $d(i)$ denotes the overall disturbance including actuator noise. Fig. 4 shows the block diagram of the design model.

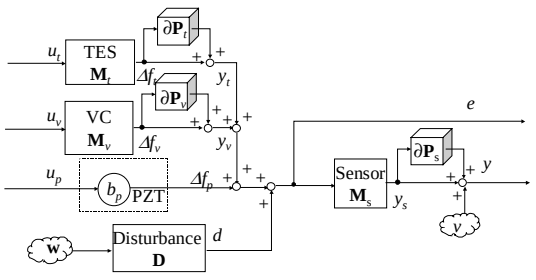

Fig. 4. Block diagram of the design model.

The controllable dynamics must be completed with the interferometer dynamics (see Section III.B) driven by $e(i)$. As control problems 2 to 4 assume interferometer to be locked-in, the sensor output $y(i)$ can be assumed to be proportional to $e(i)$ through sensor dynamics $\mathbf{M}_s$ and less the sensor noise $v(i)$ and an unmodelled dynamics $\partial\mathbf{P}_s$:

$$y(i) = y_s(i) + v(i) + \partial\mathbf{P}_s(y_s),\ y_s(i) = \mathbf{M}_s \cdot e(i). \quad (15)$$

Experimental test and analysis showed that sensor dynamics could be approximated by a single delay:

$$\mathbf{M}_s(z) = z^{-1} \quad (16)$$

2) Disturbance dynamics

Dynamics of the disturbances, being unknown, must encompass their possible realizations. This has been achieved by dynamic modeling and from experimental tests, capturing typical realizations and Power Spectral Densities (PSD). The disturbance PSD (the upper profile in Fig. 5) shows a low-frequency drift in the MBW and a resonance emerging from a faint drift beyond the MBW.

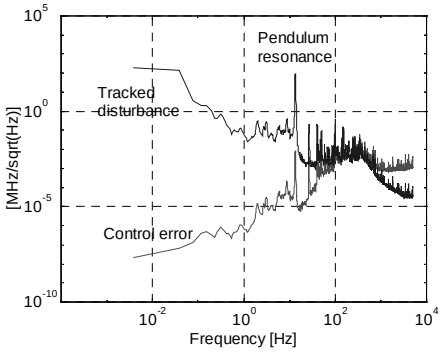

Fig. 5. PSD of disturbance and control error.

In order to track, for calibration purposes, the realizations of the experimental PSD in Fig. 5 well beyond the pendulum resonance (>100Hz), the following dynamics has been designed:

$$\begin{aligned} d(z) &= \mathbf{D} \cdot \mathbf{w}(z) = w_0(z) + \mathbf{D}_1 \cdot \mathbf{w}(z) \\ \mathbf{D}_1 \cdot \mathbf{w}(z) &= (z-1)^{-1} w_1(z) + (z-1)^{-2} w_2(z) + \\ &\quad + (z-1)^{-2}\left((z-1)^2 + \alpha(z-1) + \alpha\right)^{-1} \alpha w_3(z) \end{aligned} \quad ,(17)$$

where w_j, $j = 0,...,n_w - 1 = 3$ denotes a component of the driving noise vector $\mathbf{w}$ and α is tuned to the mean pendulum resonance $\underline{f}$. The disturbance dynamics $\mathbf{D}$ has been implemented as a 4th order DT state equation, whose states can be shown to be fully observable from y.

3) State observer

Only the state variables of the PZT-to-sensor dynamics $b_p\mathbf{M}_s$ and of the disturbance dynamics $\mathbf{D}$, for a total of $n = 5$ variables, need to be observable from the model output y. It can be shown that the dynamics of the slower actuators, TES and VC, may not be observable, being in

parallel to disturbance dynamics. As a matter of fact, (13) and (17) share the pendulum 2nd order dynamics. Indeed, their state variables need not to be either stabilized or compensated, but they just need to be forced accommodating some components of the total command.

The main goal of a state observer is to extract a suitable realization $\hat{\mathbf{w}}(i)$ of the driving noise $\mathbf{w}(i)$ from the output $y(i)$. This is obtained through an output-to-state all-pass filter $\mathbf{H}_O$ driven by the model error $e_y(i)$, the latter being defined according to (15) by

$$e_y(i) = y(i) - y_s(i). \tag{18}$$

The filter $\hat{\mathbf{w}}(i) = \mathbf{H}_O \cdot e_y(i)$ must guarantee the observer eigenvalues Λ_O to be freely assignable within the unit disk. When $n_w = n$, $\mathbf{H}_O$ can be designed to be static, but when $n_w < n$, as the present case, only a dynamic filter will guarantee free eigenvalue assignment. As $n - n_w = 1$, a 1st order dynamics driving $\hat{\mathbf{w}}$ can be shown to be necessary and sufficient to achieve asymptotic stability. Therefore the following dynamics has been designed:

$$\hat{\mathbf{w}}(z) = \mathbf{H}_O e_y(z) = \left(L_0 + L_1/(z - 1 + \gamma)\right) e_y(z), \tag{19}$$

where the vectors L_0, L_1 and the scalar γ include $n+1=6$ gains for tuning the observer eigenvalues Λ_O.

The 6th observer input-output operator $\mathbf{V}_O$ is defined by

$$\begin{aligned} y_s(z) &= \mathbf{V}_O(z)\, y(z) \\ \mathbf{V}_O(z) &= \left(1 + \mathbf{M}_s(z)\mathbf{D}(z)\mathbf{H}_O(z)\right)^{-1} \mathbf{M}_s(z)\mathbf{D}(z)\mathbf{H}_O(z) \end{aligned} \tag{20}$$

and is clearly a low-pass filter.

B. Tracking and vibration suppression

Let $\hat{d}(z) = z\mathbf{D}_1(z)\hat{\mathbf{w}}(z)$ be the one-step prediction of the disturbance realization provided by the state observer, free of $\hat{w}_0$ (see (17)) which can not be predicted. A single laser built-in actuator were available (the fastest one, the PZT) and voice coils were off, only problem 2 (and 4) could be solved by means of (i) the following simple control law

$$u_p(i) = -\hat{d}(i)/b_p, \tag{21}$$

and (ii) an appropriate Λ_O tuning so as to guarantee closed-loop stability in presence of unmodelled dynamics.

Actually TES is needed to solve Problem 1 owing to the limited PZT range, while VC actuators are available for calibration purposes. Therefore all control problems can be solved by apportioning $\hat{d}(i)$ to different actuators. Apportioning technique is the same developed in [4].

1. As defined in Section II.B, tracking and vibration suppression concerns complementary disturbance components $\hat{d}_l(i) = \mathbf{L} \cdot \hat{d}(i)$ and $\hat{d}_h(i) = (1 - \mathbf{L}) \cdot \hat{d}(i)$.
2. The low-frequency component $\hat{d}_l$ is tracked in real-time by a closed-loop dynamics $\mathbf{V}_t$ (called tracking dynamics in [4]) which is built around the TES model $\mathbf{M}_t$ and is driven by $\hat{d}_l(i)$. The input u_t to $\mathbf{M}_t$ provides the actual command to TES.
3. The same occurs to the high-frequency component $\hat{d}_h$ which is tracked by a closed-loop dynamics $\mathbf{V}_v$ built around the VC dynamics $\mathbf{M}_v$. The input u_v to $\mathbf{M}_v$ provides the actual command to VC.
4. The sum $\hat{d}_p$ of the tracking residuals defined by

$$\begin{aligned} \hat{d}_p(i) &= \hat{d}_{pl}(i) + \hat{d}_{ph}(i) = \\ &= \left(\left(1 - \mathbf{V}_t\right) \cdot \mathbf{L} + \left(1 - \mathbf{V}_t\right) \cdot \left(1 - \mathbf{L}\right)\right) \cdot \hat{d}(i) \end{aligned} \tag{22}$$

provides the actual command u_p to PZT.

The tracking dynamics $\mathbf{V}_j$, $j = t, v$ is designed to be of the form

$$\mathbf{V}_j(z) = \left(1 + \mathbf{M}_j(z)\mathbf{H}_j(z)\right)^{-1} \mathbf{M}_j(z)\mathbf{H}_j(z), \tag{23}$$

where $\mathbf{H}_j$ is a suitable feedback limiting the components to be tracked in agreement with actuator range and slew-rate (see [4]). As a result, $\mathbf{V}_t \cdot \mathbf{L}$ (TES) will be a low-pass filter with a bandwidth $f_t < f_h = 2$ Hz, while $\mathbf{V}_v \cdot (1 - \mathbf{L})$ (VC) will be a band-pass filter centered on pendulum resonance. Finally, $(1 - \mathbf{V}_t) \cdot \mathbf{L} + (1 - \mathbf{V}_v) \cdot (1 - \mathbf{L})$ (PZT) will be a band-pass filter covering from f_t to f_h and a high-pass filter covering from $f_v > \underline{f}$, so as to minimize the variance of the control error $e(i)$.

At the end, the control algorithm (see Fig. 6) solving problems 2 and 4 is the following:

$$\begin{aligned} &\hat{d}_{pl}(i) = \left(1 - \mathbf{V}_t\right) \cdot \mathbf{L} \cdot \hat{d}(i),\ u_t(i) = -\mathbf{H}_t \cdot \hat{d}_{pl}(i) \\ &\hat{d}_{ph}(i) = \left(1 - \mathbf{V}_v\right) \cdot \left(1 - \mathbf{L}\right) \cdot \hat{d}(i),\ u_v(i) = -\mathbf{H}_v \cdot \hat{d}_{ph}(i). \\ &u_p(i) = -\left(\hat{d}_{pl}(i) + \hat{d}_{ph}(i)\right)/b_p \end{aligned} \tag{24}$$

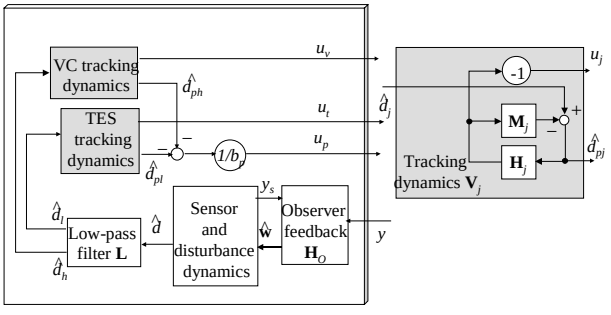

Fig. 6. Block diagram of the control algorithms.

The algorithm (24) can be shown to be equivalent to (21) if (i) unmodelled dynamics is negligible, (ii) the

eigenvalues Λ_t, Λ_v of the tracking dynamics are within the unit disk and (iii) command constraints are respected. Under the above assumptions and Λ_O lying within the unit disk, the control law (24), applied to the design model, can be shown to generate an internally stable closed-loop dynamics and therefore to solve Problem 4.

C. Closed-loop stability

Closed-loop stability in presence of unmodelled dynamics can be recovered (see [1] and [4]) by appropriate tuning of the eigenvalue sets: the observer Λ_O and the tracking dynamics Λ_v and Λ_t. First-trial tuning is performed on the basis of simple analytic models of the unmodelled dynamics $\partial\mathbf{P}_j$, $j = v,t,s$. Second-trial tuning is performed through a fine simulator of the plant dynamics. Final tuning, if necessary, is performed in-field. Eigenvalues in TABLE II correspond to in-field tuning.

TABLE II EIGENVALUES

Dynamics	Order	Eigenvalue range	Bandwidth
State observer $\mathbf{V}_O$	6	0.4÷0.95	>100 Hz
TES dynamics $\mathbf{V}_t$	3	0.9995÷0.9999	>0.1 Hz
VC dynamics $\mathbf{V}_v$	3	0.95÷0.978	>30 Hz

V. EXPERIMENTAL RESULTS

Fig. 7 shows the one-step disturbance prediction $\hat{d}(i)$, in frequency units, since interferometer lock-in occurrence at $t \cong 82$ s. The pendulum beat which is detailed in the same Figure, right, can reach 150 MHz peak-to-peak and more.

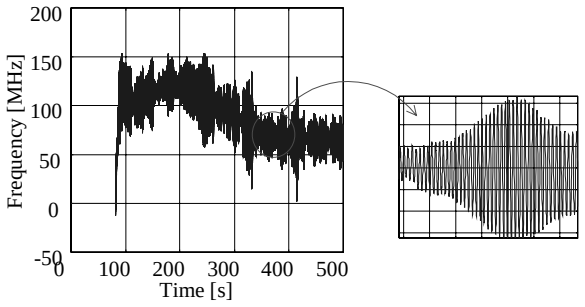

Fig. 7. Left: the estimated disturbance. Right: pendulum beat motion.

Fig. 8 shows the three digital commands compensating the disturbance of Fig. 7. All commands have been scaled to frequency units (MHz). TES command has been biased of about -600 MHz to show command overlapping. Such a command is also active during lock-in phase ($t < 82$ s) to sweep the interferometer FSR F_0 until the resonant condition (6) is found. Then the PZT quick moves the laser frequency within the linear region defined by (11) (the PZT negative peak of about 60 MHz for $t \geq 82$ s). As soon as a zero-crossing is detected (see [3]), tracking and vibration suppression start. The initial PZT offset is slowly recovered by TES, until PZT command settles around zero.

Vibration suppression is actuated by the VC command: the uniform, zero-mean strip in Fig. 8. The VC command had been absent, the PZT command would have repeated the disturbance profile in Fig. 7, reaching a peak-to-peak range of 150 MHz and even more. An enlargement of Fig. 8 would have shown the residual component of the pendulum beat to be less than 1 MHz in the PZT command, which corresponds to an attenuation factor greater than 100.

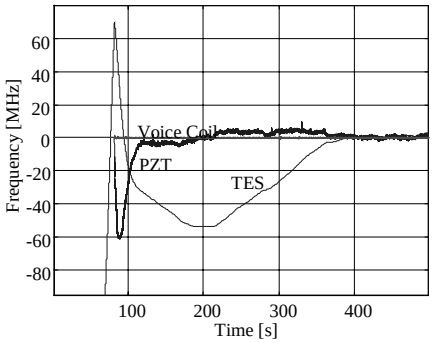

Fig. 8. The digital commands compensating the disturbance in Fig. 7.

VI. CONCLUSION

Design and experimental results of the digital control unit of the *Nanobalance* thrust-stand, centered around an active vibration suppression strategy, has been presented. Vibration suppression has the advantage of minimizing the command effort of the fastest actuator (PZT), thus preventing measurement interruptions due to command saturation because of excessive pendulum beat due to severe ground noise. The only drawback is the measurement corruption by actuator (VC) noise. Since the latter appears quite negligible with respect to instrument noise, the strategy can be employed as a back-up solution to standard one (only PZT and TES) under severe ground motion conditions.

REFERENCES

[1] Canuto E. *Controlli automatici. Parte II. Controllo digitale*. Turin, Italy: CELID, 2002 (in Italian).

[2] Canuto E., Rolino A. "Digital control of an interferometric balance for micro-thrust measurement", in *Proc. 2003 ACC*, pp. 1110-1115.

[3] Canuto E., Rolino A. "Nanobalance: an automated interferometric balance for micro-thrust measurement", *ISA Trans.*, vol. 43, no. 1, 2004.

[4] Canuto E., Rolino A. "Multi-input digital frequency stabilization of monolithic lasers", *Automatica*, to be published. See also Canuto E., Bertinetto F. "Multi-input digital frequency stabilization of metrology lasers", in *Proc. 2001 ACC*, pp. .2267-2272.

[5] Drever, R. W. et al. "Laser phase and frequency stabilization using an optical resonator". *Appl. Phys. B*, vol. 21, pp. 97-105, 1983.

[6] Orfanidis S.J. *Introduction to signal processing*. London, UK: Prentice- Hall, 1996.